

Electronic and Excitonic Structures of Inorganic–Organic Perovskite-Type Quantum-Well Crystal $(\text{C}_4\text{H}_9\text{NH}_3)_2\text{PbBr}_4$

To cite this article: Kenichiro Tanaka *et al* 2005 *Jpn. J. Appl. Phys.* **44** 5923

View the [article online](#) for updates and enhancements.

You may also like

- [Highly efficient photoluminescence of 2D perovskites enabled by dimensional increasing](#)
Linlin Ma, Chao Wang, Ya Chu et al.
- [Recent progress of the optoelectronic properties of 2D Ruddlesden-Popper perovskites](#)
Haizhen Wang, Chen Fang, Hongmei Luo et al.
- [Raman spectroscopy in layered hybrid organic-inorganic metal halide perovskites](#)
Davide Spirito, Yaiza Asensio, Luis E Hueso et al.

Electronic and Excitonic Structures of Inorganic–Organic Perovskite-Type Quantum-Well Crystal $(\text{C}_4\text{H}_9\text{NH}_3)_2\text{PbBr}_4$

Kenichiro TANAKA*, Takayuki TAKAHASHI, Takashi KONDO, Kenichi UMEDA¹, Kazuhiro EMA¹, Tsutomu UMEBAYASHI², Keisuke ASAI^{2†}, Kazuhito UCHIDA³ and Noboru MIURA³

Department of Materials Science, The University of Tokyo, 7-3-1 Hongo, Bunkyo-ku, Tokyo 113-8656, Japan

¹*Department of Physics, Sophia University, 7-1 Kioi-cho, Chiyoda-ku, Tokyo 102-8554, Japan*

²*Department of Quantum Engineering and Systems Science, The University of Tokyo, 7-3-1 Hongo, Bunkyo-ku, Tokyo 113-8656, Japan*

³*Institute for Solid State Physics, The University of Tokyo, Kashiwanoha, Kashiwa, Chiba 277-8581, Japan*

(Received January 20, 2005; accepted April 19, 2005; published August 5, 2005)

The electronic and excitonic structures of an inorganic–organic perovskite-type quantum-well crystal $(\text{C}_4\text{H}_9\text{NH}_3)_2\text{PbBr}_4$ have been investigated by optical absorption, photoluminescence, electroabsorption, two-photon absorption, and magneto-absorption spectroscopies. Excitons in $(\text{C}_4\text{H}_9\text{NH}_3)_2\text{PbBr}_4$ are of the Wannier-type, and ns ($n \geq 2$) excitons form an ideal two-dimensional Wannier exciton system. The binding energy, longitudinal–transverse splitting energy, and exchange energy of 1s excitons have been determined to be 480, 70 and 31 meV, respectively. These high values originate from both a strong two-dimensional confinement and the image charge effect. These values are larger than those in $(\text{C}_6\text{H}_{13}\text{NH}_3)_2\text{PbI}_4$, owing to the smaller dielectric constant of the well layer in $(\text{C}_4\text{H}_9\text{NH}_3)_2\text{PbBr}_4$ than that in $(\text{C}_6\text{H}_{13}\text{NH}_3)_2\text{PbI}_4$. The seemingly unusual electric-field dependence of excitons resonance is also reasonably understood by taking the image charge effect into account. [DOI: 10.1143/JJAP.44.5923]

KEYWORDS: inorganic–organic perovskite-type crystal, Wannier excitons, quantum wells, magnetoabsorption, electroabsorption, photoluminescence, two-photon absorption, two-dimensional excitons, image charge effect, quantum confinement effect

1. Introduction

In recent years, excitons confined in low-dimensional semiconductor structures have been of great interest due to their large binding energies and associated optical nonlinearities. The large family of lead-halide-based perovskite-type crystals has attracted much attention because of their unique crystal structures and optical properties. They are self-organized low-dimensional crystals, in which $[\text{PbX}_6]$ ($X = \text{I}, \text{Br}$) octahedra form zero-, one-, two or three-dimensional networks.^{1–6} Among them, $(\text{C}_n\text{H}_{2n+1}\text{NH}_3)_2\text{PbX}_4$ are two-dimensional crystals, in which excitons and charge carriers are tightly confined in monomolecular layers of $[\text{PbX}_6]$ sandwiched between organic barrier layers consisting of alkylammonium chains $[\text{C}_n\text{H}_{2n+1}\text{NH}_3]$. Owing to the intrinsically flat interfaces and very large band-gap energy differences between the adjoining layers, excitons in this group of crystals have been considered to be an ideal two-dimensional (2D) system. Another unique feature of these crystals is that the dielectric constant of the barrier layers is exceptionally smaller than that of the well layers. In such a system, one may expect to observe the so-called image charge effect,^{7–9} in which the effective Coulomb interaction between the electron and hole in the well layers is significantly enhanced. In fact, we have shown recently that (1) excitons in $(\text{C}_6\text{H}_{13}\text{NH}_3)_2\text{PbI}_4$ are of the Wannier-type,¹⁰ (2) the ns ($n \geq 2$) Wannier series are ideal 2D excitons whose binding energies are enhanced by both spatial confinement and the image charge effect, and (3) the exceptionally large binding energy of 1s excitons (361 meV) is also due to the prominent image charge effect.¹¹ Additionally, it has been found that $(\text{C}_6\text{H}_{13}\text{NH}_3)_2\text{PbI}_4$ exhibits

many unique characteristics, such as huge optical nonlinearities with ultrafast response,¹² bright electroluminescence,¹³ and outstanding scintillation characteristics.¹⁴ It has also been shown that exciton–exciton interactions play an important role in excitonic $\chi^{(3)}$ processes,¹⁵ through which the time-to-space conversion of nanojoule order femtosecond pulses with a conversion rate ≥ 140 GHz has been demonstrated.^{16,17}

On the other hand, $(\text{C}_4\text{H}_9\text{NH}_3)_2\text{PbBr}_4$ is also a 2D crystal with a larger band gap, larger effective mass, and a smaller dielectric constant of the well layers than $(\text{C}_6\text{H}_{13}\text{NH}_3)_2\text{PbI}_4$. Accordingly, excitons in $(\text{C}_4\text{H}_9\text{NH}_3)_2\text{PbBr}_4$ are expected to have a smaller Bohr radius and a larger binding energy, and thus may exhibit a larger optical nonlinearity than $(\text{C}_6\text{H}_{13}\text{NH}_3)_2\text{PbI}_4$. To fully discuss the excitonic optical nonlinearities of $(\text{C}_4\text{H}_9\text{NH}_3)_2\text{PbBr}_4$, detailed knowledge of its excitonic and electronic structures is indispensable. However, there have been few reports on the optical properties of $(\text{C}_4\text{H}_9\text{NH}_3)_2\text{PbBr}_4$.¹⁸ Our objective in this study is to clarify the electronic and excitonic structures of $(\text{C}_4\text{H}_9\text{NH}_3)_2\text{PbBr}_4$ by optical absorption, photoluminescence, electroabsorption (EA), two-photon absorption (TPA), and magnetoabsorption (MA) spectroscopies in comparison with those of $(\text{C}_6\text{H}_{13}\text{NH}_3)_2\text{PbI}_4$. We have found that $(\text{C}_4\text{H}_9\text{NH}_3)_2\text{PbBr}_4$, unlike $(\text{C}_6\text{H}_{13}\text{NH}_3)_2\text{PbBr}_4$, undergoes no structural phase transition below room temperature, retaining its crystal quality down to very low temperatures (~ 5 K). This results in $(\text{C}_4\text{H}_9\text{NH}_3)_2\text{PbBr}_4$ having sharper exciton lines than $(\text{C}_6\text{H}_{13}\text{NH}_3)_2\text{PbBr}_4$, and makes it easier to study its excitonic and electronic properties. It should be noted that, in spite of the shorter organic-layer width of $(\text{C}_4\text{H}_9\text{NH}_3)_2\text{PbBr}_4$ than that of $(\text{C}_6\text{H}_{13}\text{NH}_3)_2\text{PbBr}_4$, we expect that its excitonic and electronic structures should be essentially the same as those of $(\text{C}_6\text{H}_{13}\text{NH}_3)_2\text{PbBr}_4$, because it was reported that the optical spectra of $(\text{C}_n\text{H}_{2n+1}\text{NH}_3)_2\text{PbI}_4$ ($n = 4, 6, 8, 9, 10, 12$) are essentially the same.³

In this paper, we describe our experimental procedures in

*Present address: RIKEN, 2-1 Hirosawa, Wako, Saitama 351-0198, Japan.
E-mail address: kenichiro@riken.jp

†Present address: Department of Applied Chemistry, Tohoku University, Aramaki Aza-Aoba, Aoba-ku, Sendai 980-8579, Japan.

§2, and present results of optical absorption, photoluminescence, EA, TPA, and MA spectroscopies in §3. Section 4 is devoted to discussions, and conclusions are given in §5.

2. Experimental

We prepared single crystals and polycrystalline thin films of $(\text{C}_4\text{H}_9\text{NH}_3)_2\text{PbBr}_4$ as follows:¹⁸⁾ We first prepared $\text{C}_4\text{H}_9\text{NH}_3\text{Br}$ by reacting $\text{C}_4\text{H}_9\text{NH}_2$ with a stoichiometric amount of HBr aqueous solution at room temperature. After the reaction, the obtained solution was evaporated to remove water and washed with diethylether until the powder became white. The obtained $\text{C}_4\text{H}_9\text{NH}_3\text{Br}$ was reacted with a stoichiometric amount of PbBr_2 in dimethylformamide (DMF). $(\text{C}_4\text{H}_9\text{NH}_3)_2\text{PbBr}_4$ powder was synthesized by precipitating the obtained solution in acetone which is a poor solvent for $(\text{C}_4\text{H}_9\text{NH}_3)_2\text{PbBr}_4$. The obtained $(\text{C}_4\text{H}_9\text{NH}_3)_2\text{PbBr}_4$ powder was dissolved again in DMF, and spin-coated onto a glass substrate to prepare thin films. Since X-ray diffraction analysis showed that spin-coated films of $(\text{C}_4\text{H}_9\text{NH}_3)_2\text{PbBr}_4$ are highly oriented with the c -axis perpendicular to the substrate surfaces, the optical properties of the spin-coated films are almost identical to those of the single-crystalline samples, as measured with normal incidence. Transparent single crystals of $(\text{C}_4\text{H}_9\text{NH}_3)_2\text{PbBr}_4$ were synthesized by solvent-diffusion recrystallization from DMF solution in acetone. The single crystals were typically about $3 \times 4 \times 0.2 \text{ mm}^3$.

The reflection spectra of a $(\text{C}_4\text{H}_9\text{NH}_3)_2\text{PbBr}_4$ single crystal were measured at 5 K from 1.5 to 5.5 eV. Light from a xenon lamp made monochromatic by a spectroscope (Acton Research Corp., SP-300*i*) was focused onto the sample through a polarizer. The reflected light from the sample was detected by a photomultiplier tube (Hamamatsu Photonics Corp., R955). The Kramers–Kronig method was used to transform the reflection spectra to absorption spectra.

The polarized luminescence spectra of a $(\text{C}_4\text{H}_9\text{NH}_3)_2\text{PbBr}_4$ single crystal were taken at 5 K. The excitation light source was a frequency-doubled output of an optical parametric amplifier (Coherent Inc., RegA900) seeded by an amplified mode-lock Ti:Al₂O₃ laser (Coherent Inc., Mira 900). This excitation light source was also used in TPA spectroscopy. The excitation light had a center frequency of 3.542 eV and peak power of about 3.4 MW/cm². The wave vector k of the excitation laser was parallel to the c -axis of $(\text{C}_4\text{H}_9\text{NH}_3)_2\text{PbBr}_4$. Photoluminescences with s - and p -polarizations were detected through a polarizer set 60° to the c -axis of $(\text{C}_4\text{H}_9\text{NH}_3)_2\text{PbBr}_4$ (see inset of Fig. 3) by a CCD camera equipped with a monochromator (Acton Research Corp., SP-275). Time-resolved photoluminescence was measured using a streak camera (Hamamatsu Photonics K.K., C5680). The instrumental time resolution was about 10 ps.

EA measurements were carried out at 5 K on 100-nm-thick polycrystalline films of $(\text{C}_4\text{H}_9\text{NH}_3)_2\text{PbBr}_4$ in the “transverse” and “longitudinal” configurations, where the electric fields are applied parallel to the quantum-well layers in the transverse configuration, and perpendicular to the quantum-well layers in the longitudinal configuration, respectively. In both configurations, ac electric fields with no dc bias were applied at a frequency of 1 kHz. The sample used in the transverse configuration was a polycrystalline

film of $(\text{C}_4\text{H}_9\text{NH}_3)_2\text{PbBr}_4$ spin-coated on a glass substrate on which gold electrodes with a gap of 0.8 mm were deposited in advance. The modulated electric fields were applied across the gap between the gold electrodes. On the other hand, the sample used in the longitudinal configuration was a $(\text{C}_4\text{H}_9\text{NH}_3)_2\text{PbBr}_4$ polycrystalline film spin-coated on an ITO-deposited glass substrate, on top of which a gold electrode was deposited. The modulated electric fields were applied between ITO and the gold electrode. The sample was mounted on the sample holder in a cryostat evacuated to 10^{-5} Torr and maintained at 5 K. Light from a xenon lamp made monochromatic by a spectroscope was focused onto the sample, and the transmitted light was detected by a photomultiplier tube. The transmitted light detected by a photomultiplier tube had dc and ac components that were proportional to the transmission T and the modulated signal ΔT , respectively. The dc components were measured with a digital multimeter, while the ac components were recovered by a lock-in amplifier (NF Corp., 5610B) synchronized at twice the field frequency. We have confirmed that there was no electroluminescence in the modulated signals by checking the modulated signals when light was blocked off. The EA spectra were obtained by calculating $-\Delta T/T$ at each wavelength.

TPA measurements were carried out by illuminating the sample and monitoring exciton photoluminescence intensity (two-photon excitation spectroscopy¹⁹⁾). The wave vector k of the incident light was 30° off the c -axis of $(\text{C}_4\text{H}_9\text{NH}_3)_2\text{PbBr}_4$, and detected the photoluminescence from the sample surface. The TPA spectrum was obtained by dividing photoluminescence by the square of the laser intensity at each wavelength.

MA measurements were carried out on a $(\text{C}_4\text{H}_9\text{NH}_3)_2\text{PbBr}_4$ thin film at 4.2 K in pulsed magnetic fields up to 45 T in the Faraday configuration ($k \parallel B$), where k is the direction of the incident light and B is the magnetic field. The sample was a 100-nm-thick polycrystalline film of $(\text{C}_4\text{H}_9\text{NH}_3)_2\text{PbBr}_4$ spin-coated on a 4-mm-diameter quartz substrate. It was immersed in liquid helium in a specially designed cryostat where a coil made of Nb/Ti superconducting wires was installed in a liquid-nitrogen bath. Magnetic fields up to 45 T were generated by discharging a condenser bank into the coil. Light from a xenon lamp was introduced to the sample through an optical fiber, a polarizer and a quarter-wave plate. The light transmitted through the sample was guided through another optical fiber to an optical multi-channel analyzer (OMA). Xenon flash started at almost the same time the gate of the OMA was opened. MA spectra were taken while the gate of the OMA was open, for about 1 ms, when the magnetic field reached its peak value.

3. Results

3.1 Absorption

Figure 1 shows the optical absorption spectra of $(\text{C}_4\text{H}_9\text{NH}_3)_2\text{PbBr}_4$ at 5 K for $k \parallel c$ and $E \perp c$ configurations, where k and E are the wave vector and polarization vector of the light, respectively, and the c -axis is perpendicular to the ab -plane (layer plane). The two spectra were taken in the two configurations where the electric field E is parallel to the orthogonal crystal axes a and b . The absorption coefficient at approximately 3.75 eV in the spectrum of $E \parallel$

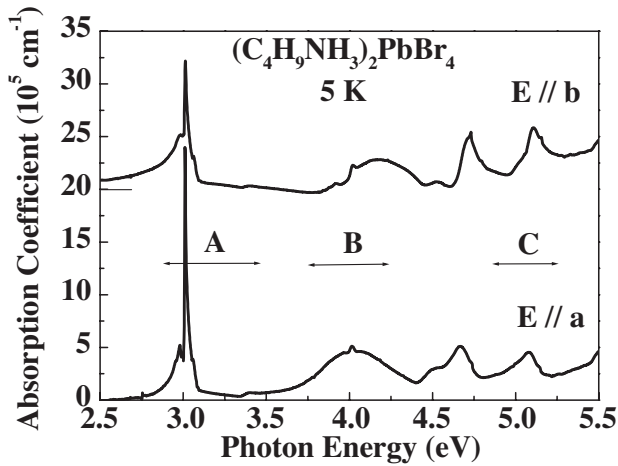


Fig. 1. Optical absorption spectra of $(\text{C}_4\text{H}_9\text{NH}_3)_2\text{PbBr}_4$ at 5 K for $E \parallel a$ and $E \parallel b$ configurations obtained by Kramers–Kronig transformation of reflection spectra. Bands A–C are discussed in the text.

b being negative may be an artifact caused by our Kramers–Kronig transformation procedure. Nevertheless, we believe that the obtained spectra are reliable, because the resonance energies of Γ_5^- excitons and the step structure at approximately 3.4 eV agree well with those determined from the absorption spectrum measured in a polycrystalline thin film of $(\text{C}_4\text{H}_9\text{NH}_3)_2\text{PbBr}_4$ [see Fig. 5(a)]. Since the optical absorption spectra of $E \parallel a$ and $E \parallel b$ configurations are essentially the same, the crystal is approximately uniaxial. The observed optical absorption spectra are similar to those of $(\text{C}_6\text{H}_{13}\text{NH}_3)_2\text{PbI}_4$,³⁾ indicating that the fundamental electronic structures of both crystals are essentially the same. The blue shift of the whole structures in $(\text{C}_4\text{H}_9\text{NH}_3)_2\text{PbBr}_4$ as compared with that in $(\text{C}_6\text{H}_{13}\text{NH}_3)_2\text{PbI}_4$ (about 0.6 eV) is due to halogen substitution.

Figure 2 shows the expansion of the optical absorption spectrum around the lowest-energy excitons in the $E \parallel a$ configuration. The prominent peak at 3.015 eV labeled Γ_5^- corresponds to the lowest-energy excitons, below which a weak peak at 2.988 eV designated Γ_1^- is observed. The Γ_1^- state is attributable to the triplet state, as will be discussed

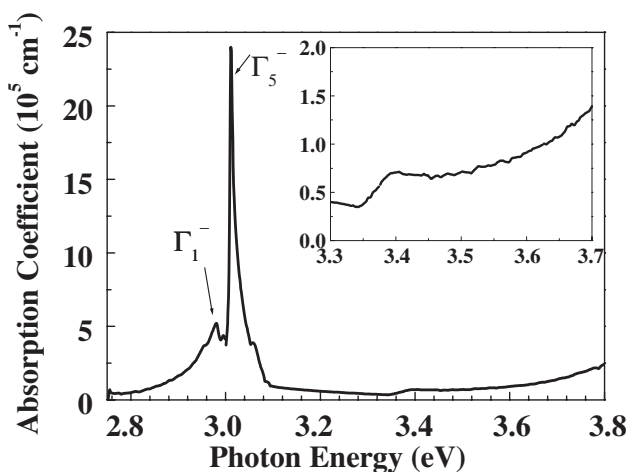


Fig. 2. Expansion of optical absorption spectra of $(\text{C}_4\text{H}_9\text{NH}_3)_2\text{PbBr}_4$ at 5 K for $E \parallel a$ configuration around the lowest-energy excitons obtained by Kramers–Kronig transformation. The inset shows expansion at approximately 3.4 eV.

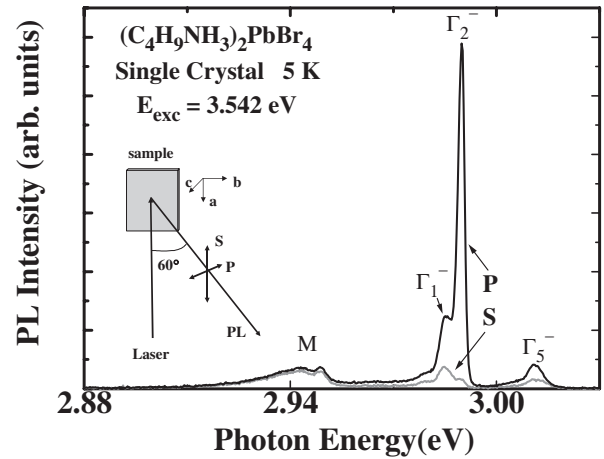


Fig. 3. Polarized luminescence spectra in single crystal of $(\text{C}_4\text{H}_9\text{NH}_3)_2\text{PbBr}_4$ at 5 K. The configuration is shown in the inset. The origins of Γ_5^- , Γ_2^- , Γ_1^- and M bands are discussed in the text.

below. Although the triplet excitons should be dipole-forbidden, they are weakly allowed by spin–orbit interactions.²⁰⁾ From the analysis of Kramers–Kronig transformation, we have determined the longitudinal–transverse splitting energy of Γ_5^- excitons to be 70 meV, which is larger than those of the lowest-energy excitons in $(\text{C}_6\text{H}_{13}\text{NH}_3)_2\text{PbI}_4$ (54 meV²¹⁾, indicating that the lowest-energy excitons in $(\text{C}_4\text{H}_9\text{NH}_3)_2\text{PbBr}_4$ have a smaller Bohr radius, larger binding energy, and a larger oscillator strength than those in $(\text{C}_6\text{H}_{13}\text{NH}_3)_2\text{PbI}_4$.

Assuming from our previous study of $(\text{C}_6\text{H}_{13}\text{NH}_3)_2\text{PbI}_4$,¹⁰⁾ we expect that ns ($n \geq 2$) excitons and band gap exist around the step structure. The inset of Fig. 2 shows the expansion of the absorption spectra around the step structure (3.40 eV), where we found no distinct peaks as observed in $(\text{C}_6\text{H}_{13}\text{NH}_3)_2\text{PbI}_4$,¹¹⁾ which may be due to the strong concentration of the oscillator strength of 1s excitons resulting in smaller oscillator strengths of ns ($n \geq 2$) excitons.

3.2 Photoluminescence

Figure 3 shows the polarized luminescence spectra of a $(\text{C}_4\text{H}_9\text{NH}_3)_2\text{PbBr}_4$ single crystal at 5 K. Free-exciton photoluminescence labeled Γ_5^- (3.010 eV) is clearly observed, under which two peaks labeled Γ_2^- (2.988 eV) and Γ_1^- (2.982 eV) were observed. We found that the Stokes shifts of Γ_5^- and Γ_1^- excitons are very small. The prominent band at approximately 2.94 eV labeled as M has been attributed to biexciton photoluminescence, i.e., a radiative recombination of a biexciton leaving an exciton behind.²²⁾ Figure 4 shows the decay curves of Γ_5^- and $\Gamma_1^- + \Gamma_2^-$ photoluminescences for a $(\text{C}_4\text{H}_9\text{NH}_3)_2\text{PbBr}_4$ single crystal at 5 K. The decay time of the $\Gamma_1^- + \Gamma_2^-$ photoluminescence (~ 10 ns) is much longer than that of Γ_5^- excitons (~ 10 ps), indicating that Γ_1^- and Γ_2^- excitons are mainly composed of triplet components, while Γ_5^- is singlet excitons, which is reasonable as is discussed in §4.1.

3.3 Electroabsorption

3.3.1 Transverse configuration

Figure 5(a) shows the optical absorption spectrum of the $(\text{C}_4\text{H}_9\text{NH}_3)_2\text{PbBr}_4$ spin-coated film at 5 K. The EA spectra

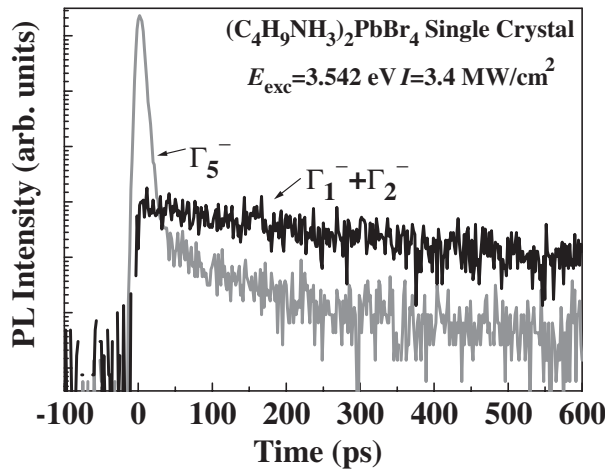


Fig. 4. Decay curves of Γ_5^- and $\Gamma_1^- + \Gamma_2^-$ photoluminescences measured at 5 K for a $(\text{C}_4\text{H}_9\text{NH}_3)_2\text{PbBr}_4$ single crystal.

under several values of electric fields in the transverse configuration are shown in Fig. 5(b). In this EA measurement, the leakage current is negligible (less than 10 nA). Clear EA signals were observed at approximately the lowest-energy excitons (3.02 eV) and at the step structures (3.40 eV). As shown in Fig. 6, the EA signal amplitudes around 3.02 eV and 3.40 eV are proportional to the square of the field strength, indicating that these EA spectra are due to the excitons.²³⁾ Figure 7(a) shows the expansion of the EA spectrum at a field strength of 29.1 kV/cm and the first derivative of the absorption spectrum with respect to the photon energy of approximately 3.02 eV. Figure 7(b) shows the expansion of the EA spectrum at a field strength of 29.1 kV/cm and the second derivative of the absorption spectrum with respect to the photon energy of approximately 3.40 eV. The EA spectra at approximately 3.02 eV are attributable to the Stark shift of the lowest-energy excitons, while the EA spectra at approximately 3.40 eV are attributed to the life-time broadening of the 2s excitons, because the EA spectrum at approximately 3.02 and 3.40 eV exhibits first-derivative and second-derivative shapes of the absorption spectra, respectively.^{10,23)} Since these characteristics are the same as those of the EA spectra in $(\text{C}_6\text{H}_{13}\text{NH}_3)_2\text{PbI}_4$, we conclude that the excitonic internal structures of $(\text{C}_4\text{H}_9\text{NH}_3)_2\text{PbBr}_4$ are essentially the same as those of $(\text{C}_6\text{H}_{13}\text{NH}_3)_2\text{PbI}_4$; i.e., they are Wannier excitons.

3.3.2 Longitudinal configuration

Figure 5(c) shows the EA spectra at several electric fields in the longitudinal configuration. The leakage current is also negligible (less than 10 nA) in the longitudinal configuration. We found that the EA spectra in the longitudinal configuration are qualitatively different from those in the transverse configuration, indicating that excitons in this crystal have very strong 2D characteristics. The striking differences are summarized as follows: (1) The lifetime broadening of 2s excitons observed in the transverse configuration is not observed in the longitudinal configuration, even though the applied electric field in the longitudinal configuration is about 35 times as large as that in the transverse one. This is because a barrier layer impedes the ionization of 2s excitons, as is observed in the so-called quantum-confined Stark effect

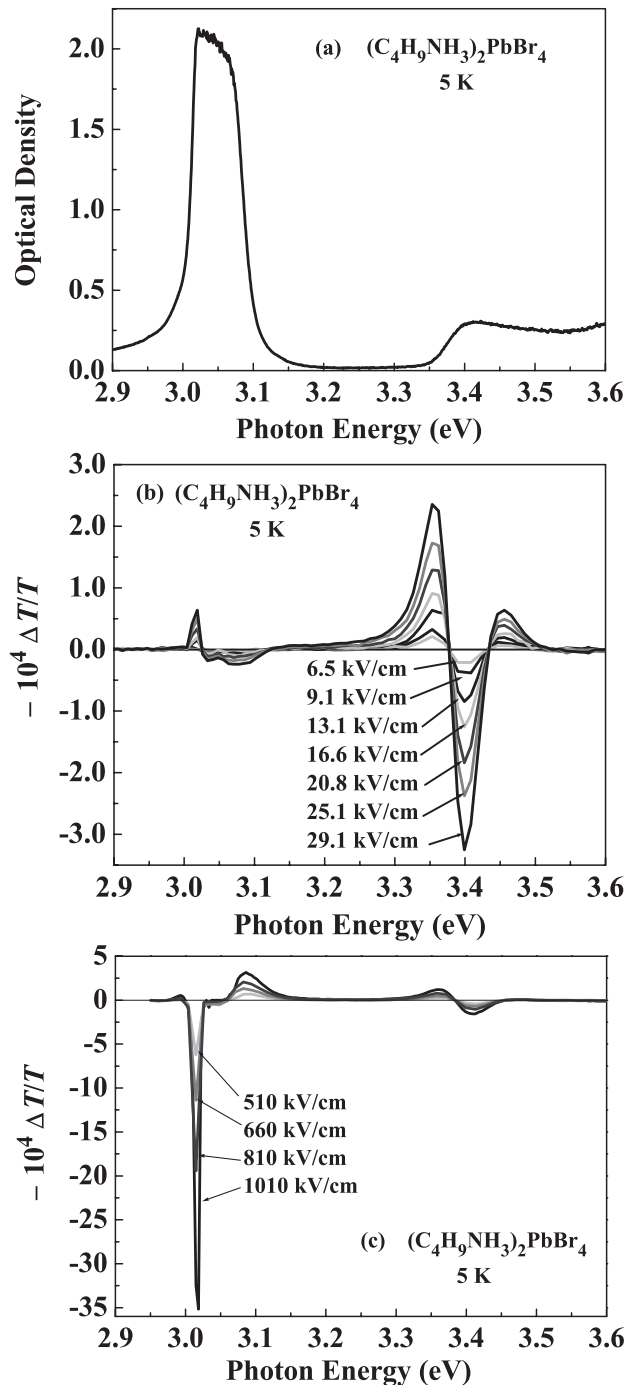


Fig. 5. (a) Optical absorption spectrum, (b) EA spectra at several electric fields in the transverse configuration, and (c) EA spectra at several electric fields in longitudinal configuration of $(\text{C}_4\text{H}_9\text{NH}_3)_2\text{PbBr}_4$ spin-coated film at 5 K.

(QCSE).²⁴⁾ In addition, the EA spectra show the redshift of 2s excitons and the blueshift of 1s excitons, which are justified because the EA spectra around the 1s and 2s excitons agree well in shape with the sign reversal of the first derivative and the first derivative of the optical absorption spectrum, respectively. The measured shifts of the 1s and 2s excitons peaks as functions of electric field are shown by the closed and open circles in Fig. 8, respectively. Here, the absolute values of the shifts, ΔE , were obtained using

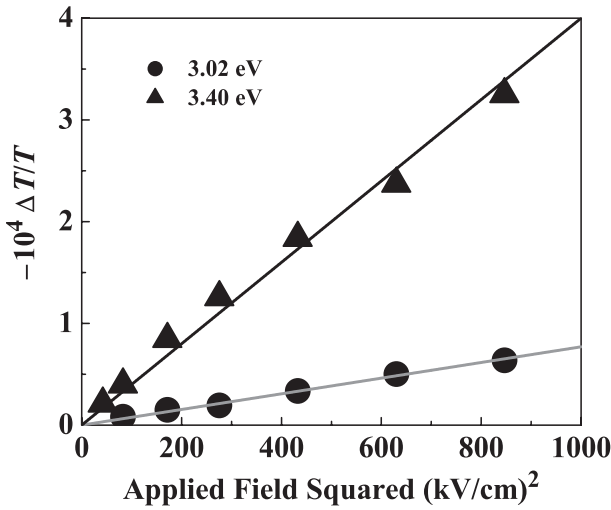


Fig. 6. Electric field dependence of EA signal amplitudes of positive peak at 3.02 eV and negative peak at 3.40 eV in transverse configuration.

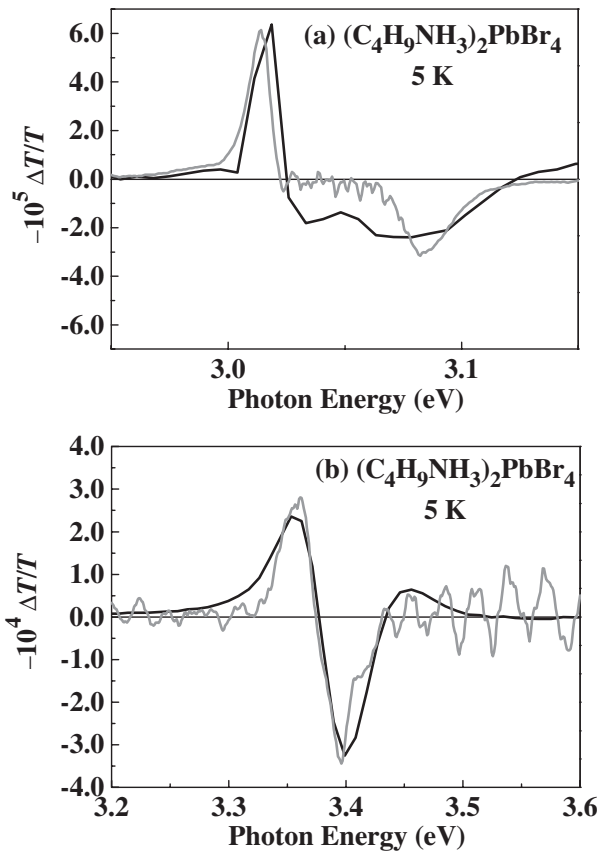


Fig. 7. (a) Transverse EA spectrum at field strength of 29.1 kV/cm (black line) and first derivative of absorption spectrum at approximately 3.02 eV. (b) Transverse EA spectrum at field strength of 29.1 kV/cm (black line) and second derivative of absorption spectrum (gray line) at approximately 3.40 eV.

$$-\frac{\Delta T}{T} = \ln 10 \frac{d(\text{OD})}{dE} \Delta E, \quad (1)$$

where OD is the optical density, and E is the photon energy. The observed blue shift of the 1s excitons seems a unique behavior, because in conventional semiconductor quantum wells, electric fields perpendicular to the well layers pull the

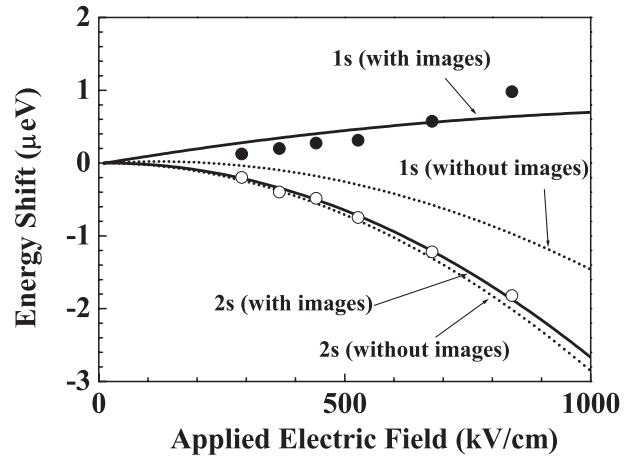


Fig. 8. Energy shifts of 1s and 2s exciton peaks in the longitudinal configuration as a function of the applied electric field. Closed and open circles represent the experimental values for 1s and 2s, and the lines represent the theoretical calculation with (solid) and without (dashed) consideration of the image charge effect.

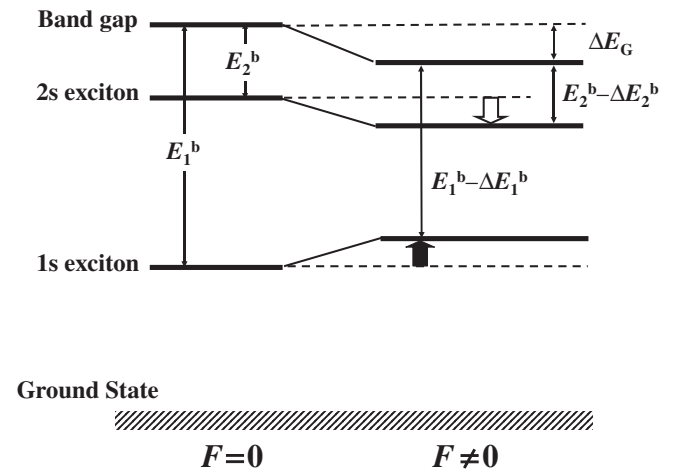


Fig. 9. Schematic illustration of energy levels of band gap, and 1s and 2s excitons in $(\text{C}_4\text{H}_9\text{NH}_3)_2\text{PbBr}_4$ without ($F = 0$) and with ($F \neq 0$) external electric field in longitudinal configuration.

electrons and holes towards opposite sides of the layers, usually resulting in a large reduction in band-gap energy and a small reduction in exciton binding energy, thus corresponding to a *redshift* of the exciton peak (QCSE).²⁴⁾

Figure 9 illustrates the mechanism of the seemingly unusual behavior of excitons.¹¹⁾ The band gap is redshifted by ΔE_G (>0) under the applied electric fields. On the other hand, the 1s and 2s excitons binding energies are reduced by ΔE_1^b (>0) and ΔE_2^b (>0), respectively, owing to the electric-field-induced separation between the electron and the hole. The direction and amount of the energy shift of the exciton resonance energy are determined according to the relative magnitudes of the band-gap redshift (ΔE_G) and the reduction in the binding energy of excitons (ΔE_1^b and ΔE_2^b). Since the 2s excitons have a larger Bohr radius, the electric-field-induced change in the distance between the electron and the hole has a smaller influence on their binding energy, i.e., ΔE_2^b should be relatively smaller. On the other hand, since the 1s excitons have a smaller Bohr radius, the

electric-field-induced change in the distance between the electron and the hole results in a larger reduction in their binding energy. That is, ΔE_1^b should be relatively larger. We supposed that $\Delta E_2^b < \Delta E_G < \Delta E_1^b$ in this case, resulting in the redshift of the 2s excitons and the blue shift of the 1s ones. This assumption will be justified by our quantitative argument in §4.2.2.

On the other hand, we found that the EA signals above 3.50 eV are completely suppressed. The same behavior was also observed in the EA spectra of $(C_6H_{13}NH_3)_2PbI_4$ in the longitudinal configuration above the band gap (2.700 eV), indicating that the carriers in $(C_6H_{13}NH_3)_2PbI_4$ are tightly confined two-dimensionally.^{5,11)} We thus assumed that the band gap of $(C_4H_9NH_3)_2PbBr_4$ is located at 3.50 eV, from which the binding energies of the 1s and 2s excitons are estimated to be 480 and 100 meV, respectively. Here, it should be noted that the binding energy of the 1s exciton is at least 6 times larger than that of the three-dimensional (3D) analogue $CH_3NH_3PbBr_3$ (76 meV²⁵⁾). Since the spatial confinement only quadruples the exciton binding energy in the 2D limit,²⁶⁾ this strong enhancement factor (>6) indicates that the image charge effect definitely increases exciton binding energy.

3.4 Two-photon absorption

Figure 10(a) shows the TPA spectrum of a $(C_4H_9NH_3)_2PbBr_4$ single crystal at 5 K. The excitation light intensity was on the order of several kW/cm². In the excitation power range, we found no biexciton photoluminescence. Figure 10(b) shows the typical photoluminescence spectrum when the incident-light photon energy and power were 1.702 eV and 200 kW/cm², respectively. We found only Γ_2^- exciton photoluminescence, which was proportional to the square of the incident light intensity, as shown in the inset of Fig. 10(b). We therefore determined the TPA coefficient by monitoring the photoluminescence intensity of Γ_2^- excitons at 2.988 eV.

In the TPA spectrum of $(C_4H_9NH_3)_2PbBr_4$ [Fig. 10(a)], we found a clear resonance peak at 3.406 eV, which is attributable to the 2p state of the Wannier series, because the resonance energy is nearly equal to that of the 2s state observed in the EA spectrum.

3.5 Magnetoabsorption

Figure 11 shows the MA spectra around the 1s excitons of $(C_4H_9NH_3)_2PbBr_4$ in the Faraday configuration for the left-handed circular (σ^-) polarization. The MA spectrum for the right-handed polarization is displayed only for the highest magnetic field by a dashed line for comparison. The magnetic-field-induced energy shifts were very small, which indicates that the 1s excitons in $(C_4H_9NH_3)_2PbBr_4$ have a very small Bohr radius. The peak energies of the lowest-energy excitons are plotted as functions of magnetic field, by closed circles for σ^+ , and open circles for σ^- polarizations in Fig. 12.

The solid line in Fig. 12 are theoretical curves fitted with the method of least squares by

$$E = E_0 \pm \frac{1}{2} g_{\perp} \mu_B B + c_0 B^2, \quad (2)$$

where E_0 is the energy of the absorption peak at 0 T, g_{\perp} the

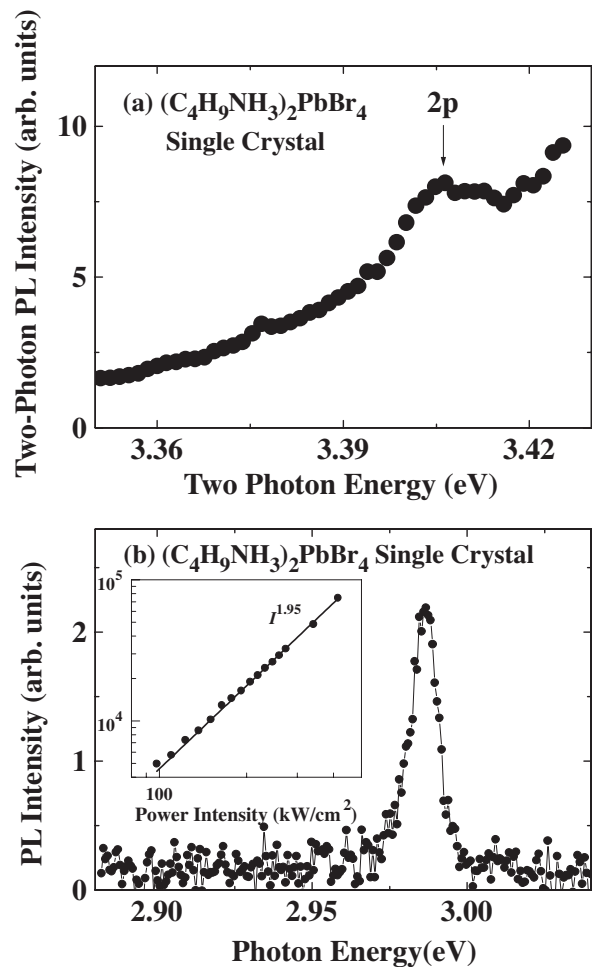


Fig. 10. (a) Two-photon absorption spectrum of $(C_4H_9NH_3)_2PbBr_4$ single crystal at 5 K. (b) Photoluminescence spectrum where excitation photon energy and power are 1.702 eV and 200 kW/cm², respectively. Biexciton photoluminescence is not observed. The inset shows the excitation power dependence of Γ_2^- photoluminescence at 2.988 eV.

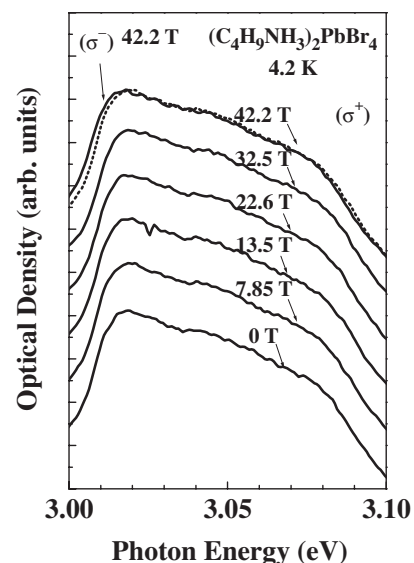


Fig. 11. Magnetoabsorption spectra of $(C_4H_9NH_3)_2PbBr_4$ in Faraday configuration at 4.2 K. The spectra are shown for σ^+ polarization (solid lines) and σ^- polarization (dashed line).

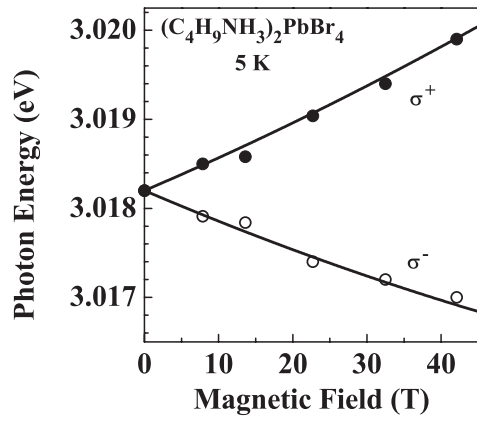


Fig. 12. Energy shifts as functions of magnetic field in Faraday configuration. Closed circles and open circles represent the experimental values for σ^+ and σ^- polarizations, and solid lines show the theoretical fitting obtained by the least-squares method.

effective g factor perpendicular to the ab -plane, c_0 the diamagnetic coefficient, and μ_B the Bohr magneton. The second term of eq. (2) is the Zeeman term and the third term is the diamagnetic shift. From the fitting, we have obtained $g_{\perp} = 1.2$ and $c_0 = (1.2 \pm 0.3) \times 10^{-7} \text{ eV/T}^2$.

4. Discussion

4.1 Electronic and excitonic structures

The electronic and excitonic structures of $(\text{C}_4\text{H}_9\text{NH}_3)_2\text{PbBr}_4$ have been analyzed in terms of group theoretical considerations (see Fig. 13). Although the point group of $(\text{C}_4\text{H}_9\text{NH}_3)_2\text{PbBr}_4$ crystal is C_{2v} ,¹⁸⁾ we approximately take the symmetry of $(\text{C}_4\text{H}_9\text{NH}_3)_2\text{PbBr}_4$ as tetragonal (D_{4h}) for simplicity, because this crystal is approximately uniaxial. A first-principles band calculation shows that the lowest

unoccupied (LUMO) states of $[\text{PbBr}_6]$ octahedron are composed of the σ antibonding of $\text{Pb}(6p)\text{-Br}(4s)$ and π antibonding orbitals, and that the highest-occupied (HOMO) states are decomposed into three parts as described in our previous paper, the top of which is composed of σ antibonding of $\text{Pb}(6s)\text{-Br}(4p)$ orbitals.²⁷⁾ Here, we found that the LUMO and HOMO states of a $[\text{PbBr}_6]$ octahedron have Γ_4^- and Γ_1^+ symmetries in the point group of the $[\text{PbBr}_6]$ octahedron (O_h). After introducing the spin-orbit interactions and tetragonal crystal field, the HOMO state transforms to Γ_6^+ ($J_z = \pm 1/2$), while the LUMO state splits into three bands (A–C), where both A and C have Γ_6^- symmetry ($J_z = \pm 1/2$), and B has Γ_7^- ($J_z = \pm 3/2$) symmetry. Here, J_z is the z component of the total angular momentum J . As was shown by Ishihara *et al.*, these three bands A–C are attributable to the optical absorption spectra shown in Fig. 1.³⁾ From the energy separations in the absorption spectrum, we have obtained the crystal-field parameter $T = -0.513 \text{ eV}$ and spin-orbit parameter $\lambda = -0.380 \text{ eV}$, which are close to those of $(\text{C}_6\text{H}_{13}\text{NH}_3)_2\text{PbI}_4$ ($T = -0.505 \text{ eV}$, $\lambda = -0.322 \text{ eV}$).⁴⁾ This denotes that the electronic structures of $(\text{C}_4\text{H}_9\text{NH}_3)_2\text{PbBr}_4$ are essentially the same as those of $(\text{C}_6\text{H}_{13}\text{NH}_3)_2\text{PbI}_4$.

Here we only discuss the structures of the lowest-energy excitons (A). The excitons in the other bands can be analyzed in the same way. The lowest-energy excitons comprise three exciton levels that have $\Gamma_1^-, \Gamma_2^-,$ and Γ_5^- symmetries and thus have different optical selection rules, because the direct product $\Gamma_6^+ \times \Gamma_6^-$ transforms according to $\Gamma_1^- + \Gamma_2^- + \Gamma_5^-$ representations. Here, the Γ_1^- ($J_z = 0$) exciton is a pure spin triplet and thus dipole-forbidden, and the Γ_2^- ($J_z = 0$) exciton is observable in the $E \parallel c$ configuration; twofold Γ_5^- ($J_z = \pm 1$) excitons are observable in the $E \perp c$ configuration. The Γ_2^- exciton is composed of mainly triplet excitons, and thus its oscillator strength is relatively small; on the other hand, the Γ_5^- exciton is mainly a singlet exciton, and hence its oscillator strength is larger. These excitons are split by the exchange interactions between the electron and the hole. The excitons wave functions with $\Gamma_1^-, \Gamma_2^-,$ and Γ_5^- symmetries are described as

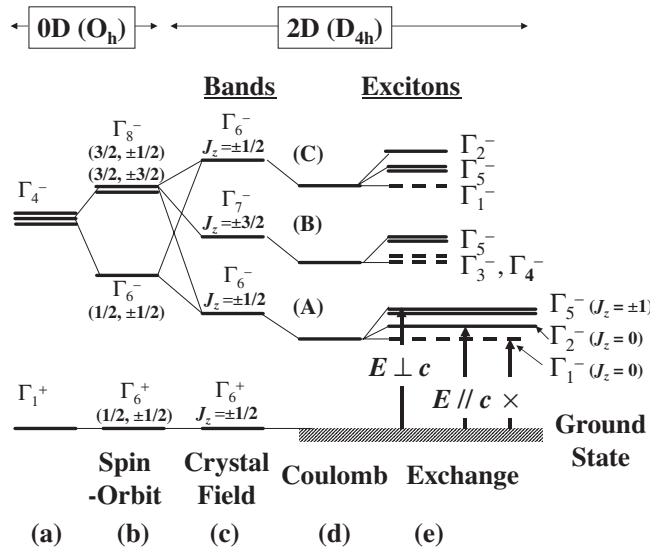


Fig. 13. Schematic energy diagram of two-dimensional crystal $(\text{C}_4\text{H}_9\text{NH}_3)_2\text{PbBr}_4$ at Γ point of Brillouin zone. (a) The LUMO and HOMO states of the $[\text{PbBr}_6]$ octahedron have Γ_4^- and Γ_1^+ symmetries, respectively. (b) With spin-orbit interaction and (c) tetragonal crystal field, the LUMO state splits into the three bands A, B, and C, while the HOMO state is not split. The excitons in each band are split by the (d) Coulomb and (e) exchange interactions. Only the selection rules to the lowest-energy excitons (A band) are described.

$$\phi^1 = \frac{1}{\sqrt{2}} (P_{+e} S_h \beta_e \alpha_h - P_{-e} S_h \alpha_e \beta_h) \cos \theta - \frac{1}{\sqrt{2}} P_{0e} S_h (\alpha_e \alpha_h - \beta_e \beta_h) \sin \theta \quad \text{for } \Gamma_1^-, \quad (3)$$

$$\phi^2 = \frac{1}{\sqrt{2}} (P_{+e} S_h \beta_e \alpha_h + P_{-e} S_h \alpha_e \beta_h) \cos \theta - \frac{1}{\sqrt{2}} P_{0e} S_h (\alpha_e \alpha_h + \beta_e \beta_h) \sin \theta \quad \text{for } \Gamma_2^-, \quad (4)$$

$$\phi_+^5 = P_{+e} S_h \beta_e \beta_h \cos \theta - P_{0e} S_h \alpha_e \beta_h \sin \theta \quad \text{for } \Gamma_5^-, \quad (5)$$

$$\phi_-^5 = P_{-e} S_h \alpha_e \alpha_h \cos \theta - P_{0e} S_h \beta_e \alpha_h \sin \theta \quad \text{for } \Gamma_5^-, \quad (6)$$

$$\tan 2\theta = \frac{2\sqrt{2}\lambda}{\lambda + 3T}, \quad \left(0 \leq \theta \leq \frac{\pi}{2} \right), \quad (7)$$

where S is the wave function of the HOMO state of the $[\text{PbBr}_6]$ octahedron; P_+ , P_0 , and P_- are the wave functions of the LUMO state of the $[\text{PbBr}_6]$ octahedron, in which +, 0, and - indicate the z components of its angular momentum being 1, 0, and -1, respectively; e and h are the electron and hole states, respectively; and α and β indicate the up and

down spins, respectively. From eq. (7) and $\lambda = -0.380$ eV and $T = -0.513$ eV, we obtained $\sin \theta = 0.320$. The excitons resonance energies with Γ_1^- , Γ_2^- , and Γ_5^- symmetries are

$$E_1 = E_A - v \quad \text{for } \Gamma_1^-, \quad (8)$$

$$E_2 = E_A - v + 2w \sin^2 \theta \quad \text{for } \Gamma_2^-, \quad (9)$$

$$E_5 = E_A - v + w \cos^2 \theta \quad \text{for } \Gamma_5^-, \quad (10)$$

where v is the Coulomb integral and w the exchange integral.^{4,28)} Here, the long-range part of the exchange interactions between the electron and the hole are neglected, because the transverse excitons are unaffected by the long-range exchange interaction when the excitons are delocalized Wannier excitons, which amount to the neglect of local-field corrections.²⁹⁾

The photoluminescence from these exciton states to the ground state are observed and attributed to Γ_1^- , Γ_2^- , and Γ_5^- in Fig. 3, which is justified for the following reasons: (1) Γ_2^- exciton photoluminescence is mainly polarized as $\mathbf{E} \parallel c$. (2) The decay time of the $\Gamma_1^- + \Gamma_2^-$ photoluminescence is much longer than that of Γ_5^- excitons, indicating that Γ_1^- and Γ_2^- excitons are mainly composed of triplet excitons, and are not bound excitons, because bound excitons should decay as fast as Γ_5^- excitons should. (3) E_1 should be the smallest among E_1 , E_2 , and E_5 .

Here, we present the following comments: (1) Based on optical selection rules, Γ_2^- excitons cannot be observed in the photoluminescence spectrum with s-polarization. We suppose that the observed Γ_2^- photoluminescence with s-polarization is caused by a misalignment of the polarizer in front of the detector. (2) Although Γ_2^- excitons have a much smaller oscillator strength than Γ_5^- excitons, the former's photoluminescence is much stronger than the latter's. This is because most excited Γ_5^- excitons decay to Γ_2^- excitons, after which they recombine themselves.³⁰⁾

From the photoluminescence peaks $E_1 = 2.982$ eV, $E_2 = 2.988$ eV, $E_5 = 3.010$ eV with eq. (8)–(10), we deduced $\sin \theta = 0.32$ and an exchange energy $w = 31$ meV. It was confirmed that the obtained $\sin \theta$ agrees well with the obtained value from eq. (7) (0.320). The obtained w is much larger than those of the lowest-energy excitons in conventional semiconductors (for example: 20 μ eV in GaAs,³¹⁾ 0.1 meV in ZnSe,³²⁾ 7 meV in CuCl³³⁾, and is still larger than that of the 1s excitons in $(\text{C}_6\text{H}_{13}\text{NH}_3)_2\text{PbI}_4$ (12 meV).²¹⁾ The huge w indicates that the spatial confinement and image charge effect make the excitons' Bohr radius smaller, resulting in a larger overlap of the electron and hole. The larger w in $(\text{C}_4\text{H}_9\text{NH}_3)_2\text{PbBr}_4$ than in $(\text{C}_6\text{H}_{13}\text{NH}_3)_2\text{PbI}_4$ is due to the smaller Bohr radius of the former than the latter.

4.2 Image charge effect

4.2.1 Exciton binding energies

We calculated the ns exciton binding energies E_n^b (>0) based on Muljarov's formalism.³⁴⁾ We solved the 2D Schrödinger equation describing the in-plane excitons motion.

$$-\frac{\hbar^2}{2\mu} \left(\frac{d^2}{d\rho^2} + \frac{1}{\rho} \frac{d}{d\rho} - \frac{m^2}{\rho^2} \right) R_m(\rho) + V(\rho)R_m(\rho) = -E_n^b R_m(\rho), \quad (11)$$

Here, μ is the reduced mass of the in-plane motion of an exciton, and m and $R_m(\rho)$ are the exciton angular momentum and in-plane wave function, respectively.

$$V(\rho) = \int dz_e \int dz_h |\psi^e(z_e)|^2 |\psi^h(z_h)|^2 V(z_e, z_h, \rho) \quad (12)$$

$V(\rho)$ is the averaged image-charge-mediated potential. Here, $V(z_e, z_h, \rho = |\rho_e - \rho_h|)$ represents the electrostatic potential at point (ρ_e, z_e) made by a hole located at (ρ_h, z_h) ; $\psi^e(z_e)$ and $\psi^h(z_h)$ are one-electron and hole wave functions for the direction perpendicular to the quantum well layers, respectively. We have shown recently that effective mass approximation is not appropriate for describing the motions of electrons and holes in the direction perpendicular to the quantum well layers, because the quantum well layers are composed of only one $[\text{PbX}_6]$ layers.⁵⁾ Accordingly the most reasonable $\psi^{e,h}(z)$ we should use to evaluate eq. (12) are the HOMO and LUMO of a $[\text{PbBr}_6]$ octahedron that have been obtained by our first-principles calculations.²⁷⁾ However, to avoid tedious calculations, we chose the simplest step functions: $\psi^{e,h} = 1/\sqrt{l_w}$ (in the well), 0 (outside the well), where l_w is the width of the well layer. In spite of this rather crude simplification, the obtained results satisfactorily reproduce the experimental results, as will be shown below. In this calculations, we used l_w and μ as adjustable parameters under the condition $l_w + l_b = (5.9 + 8.1) \text{ \AA}$,¹⁸⁾ where l_b is the width of the barrier layer; we set $\varepsilon_w = 4.8$ ²⁵⁾ and $\varepsilon_b = 2.1$,³⁾ where ε_w and ε_b are the high-frequency dielectric constants of the well layer and the barrier layer, respectively. The reason high-frequency dielectric constants are used is that when the binding energy of the exciton is much higher than the energy of the optical phonons, the relative motion of the electron and hole is too fast for the optical phonons to follow.⁴⁾ We also calculated the diamagnetic coefficient of the 1s excitons c_0 from their wave function Ψ with the formula $c_0 = (e^2/8\mu) \langle \Psi | \rho^2 | \Psi \rangle$ to fit the experimental data $[(1.2 \pm 0.3) \times 10^{-7} \text{ eV/T}^2]$. The calculated E_1^b , E_2^b and c_0 were fitted to the experimental data.

The fitting was satisfactory. We obtained $E_1^b = 470$ meV, $E_2^b = 92$ meV, and $c_0 = 1.4 \times 10^{-7} \text{ eV/T}^2$ for $\mu = 0.17m_0$, $l_w = 5.0 \text{ \AA}$. Since the obtained μ is nearly equal to that of $(\text{C}_6\text{H}_{13}\text{NH}_3)_2\text{PbI}_4$ ($0.18m_0$), the remarkably larger excitons binding energies of $(\text{C}_4\text{H}_9\text{NH}_3)_2\text{PbBr}_4$ than those of $(\text{C}_6\text{H}_{13}\text{NH}_3)_2\text{PbI}_4$ mainly originates from the smaller dielectric constant of the well layers, while the difference between their excitons' reduced masses has a minor effect on their binding energy. The calculated Bohr radius of the 1s excitons is 12 \AA , which is smaller than that of excitons in $(\text{C}_6\text{H}_{13}\text{NH}_3)_2\text{PbI}_4$ (14 \AA).¹¹⁾ This is reasonable because the dielectric constant of the well layer in $(\text{C}_4\text{H}_9\text{NH}_3)_2\text{PbBr}_4$ is smaller than that in $(\text{C}_6\text{H}_{13}\text{NH}_3)_2\text{PbI}_4$. On the other hand, the obtained μ is slightly larger than that of the lowest-energy exciton in the $\text{CH}_3\text{NH}_3\text{PbBr}_3$ ($0.13m_0$),²⁵⁾ which is consistent with our recent band calculation.²⁷⁾ For comparison, we calculated $E_1^b = 176$ meV (for $\mu = 0.17m_0$) when the image charge effect is not taken into account ($\varepsilon_b = \varepsilon_w = 4.8$), which is about 2.3 times as large as the binding energy of the lowest-energy excitons in the three-dimensional analogue $\text{CH}_3\text{NH}_3\text{PbBr}_3$ (76 meV²⁵⁾). Since the spatial confinement enhances the 1s exciton binding energy by four times in the 2D limit, this enhancement factor 2.3

(<4) indicates that the in-plane 1s exciton Bohr radius is *not* significantly larger than the perpendicular Bohr radius (well width). Nevertheless, it is worth noting that the 1s exciton binding energy (480 meV) is still at least 6 times as large as that in the three dimensional analogue $\text{CH}_3\text{NH}_3\text{PbBr}_3$. This additional enhancement factor ($6/2.3 \sim 2.6$) is definitely due to the image charge effect, which is much larger than the image charge enhancement reported for excitons in near-surface $\text{In}_x\text{Ga}_{1-x}\text{As}/\text{GaAs}$ quantum wells (~ 1.5).³⁵⁾ The following are also worth noting: (1) The enhancement factor (~ 6) of the 1s exciton binding energy in $(\text{C}_4\text{H}_9\text{NH}_3)_2\text{PbBr}_4$ is smaller than that in $(\text{C}_6\text{H}_{13}\text{NH}_3)_2\text{PbI}_4$ (~ 7).¹¹⁾ This is reasonable because the dielectric constant difference between the well layer and the barrier layer is smaller in $(\text{C}_4\text{H}_9\text{NH}_3)_2\text{PbBr}_4$ than in $(\text{C}_6\text{H}_{13}\text{NH}_3)_2\text{PbI}_4$. (2) In spite of the smaller enhancement factor due to the image charge effect, the exciton binding energy of the 1s excitons in $(\text{C}_4\text{H}_9\text{NH}_3)_2\text{PbBr}_4$ is much larger than that in $(\text{C}_6\text{H}_{13}\text{NH}_3)_2\text{PbI}_4$. This is also reasonable because the dielectric constant of the well layer is smaller in $(\text{C}_4\text{H}_9\text{NH}_3)_2\text{PbBr}_4$.

On the other hand, we calculated $E_2^b = 32$ meV when the image charge effect is not taken into account ($\varepsilon_w = \varepsilon_b = 4.8$). Since the binding energy of the 2s exciton in $\text{CH}_3\text{NH}_3\text{PbBr}_3$ is estimated to be $76 \times 1/4 = 19$ meV, the theoretical $E_2^b = 19 \times 16/9 = 34$ meV in the 2D limit²⁶⁾ when the image charge effect is not taken into account. This value agree well with the calculated $E_2^b = 32$ meV, indicating that the 2s excitons are ideal 2D excitons confined tightly. From these calculations, we conclude that (1) the ns ($n \geq 2$) excitons in $(\text{C}_4\text{H}_9\text{NH}_3)_2\text{PbBr}_4$ are sufficiently confined, and thus their binding energies are sufficiently enhanced due to both the 2D spatial and image charge effect, and that (2) although these effects are insufficient for the 1s exciton with a smaller Bohr radius, its binding energy is still substantially enhanced, which are the same as that of $(\text{C}_6\text{H}_{13}\text{NH}_3)_2\text{PbI}_4$.

4.2.2 Electric field effect

In §3.3.2, we have suggested that a blue shift of the 1s excitons observed in the EA spectra in the longitudinal configuration occurs because the magnitude of the reduction in exciton binding energy exceeds that of the band-gap redshift. To justify our assumption, we calculated the shifts of E_1^{res} and E_2^{res} under electric fields by the following procedure: (i) We estimated the polarizabilities of the HOMO and LUMO states of the $[\text{PbBr}_6]$ octahedron. The polarizability of the HOMO α_S^{H} was calculated by *ab-initio* molecular orbital calculations using the B-LYP method³⁶⁾ and the CEP-31G basis sets.³⁷⁾ We performed these calculations using the Gaussian 98 code,³⁸⁾ and obtained $\alpha_S^{\text{H}} = 25.2 \text{ \AA}^3$. On the other hand, since we could not calculate the polarizability of the LUMO α_S^{L} by the same code, we tentatively assume $\alpha_S^{\text{L}} \sim \alpha_S^{\text{H}}$, the validity of which will be confirmed later. (ii) Assuming that $\psi^{e,h}(z)$ are linear functions polarized along the perpendicular direction to the quantum well layers, we calculated $V(\rho)$ using eq. (12). (iii) We calculated E_1^b , E_2^b and their changes (ΔE_1^b , $\Delta E_2^b > 0$) by solving eq. (11). In this calculation, we neglected the self energies of the electron and hole that give a minor contribution.³⁹⁾

The calculation showed that (a) both E_1^b and E_2^b are

reduced under electric fields, with the calculated $|\Delta E_1^b - \Delta E_2^b|$ nearly identical with the measured $|\Delta E_1^{\text{res}} - \Delta E_2^{\text{res}}|$, where $\Delta E_1^{\text{res}} (>0)$ and $\Delta E_2^{\text{res}} (<0)$ are the magnitudes of the shifts of the 1s and 2s excitons resonance energies, respectively. (b) ΔE_1^b is much larger than ΔE_2^b ($\Delta E_1^b \sim 15\Delta E_2^b$), which is quite reasonable because the 1s excitons have a smaller in-plane Bohr radius, and thus the field-induced separation of the electron and hole has a larger influence on their binding energy. (c) ΔE_2^b is much smaller than the magnitude of the measured 2s exciton shift, indicating that the observed energy shift of the 2s exciton is mainly due to that of the band gap. The magnitude of the band-gap shift is reasonable in the following order-of-magnitude arguments. The band-gap shift under the electric field F is given by $-(1/2)(\alpha_S^{\text{L}} - \alpha_S^{\text{H}})F^2$; from the measured 2s exciton shift, we estimate $(\alpha_S^{\text{L}} - \alpha_S^{\text{H}}) \sim 0.9 \text{ \AA}^3$. Since the HOMO and LUMO states of a $[\text{PbBr}_6]$ octahedron are mainly composed of $\text{Pb}(6s)^2$ and $\text{Pb}(6s)(6p)$,²⁷⁾ and their electron configurations are the same as the 6^1S_0 and 6^3P_1 states of Hg atoms, we believe that $(\alpha_S^{\text{L}} - \alpha_S^{\text{H}})$ should be nearly equal to $\alpha_0(^3\text{P}_1) - \alpha_0(^1\text{S}_0)$, where $\alpha_0(^3\text{P}_1)$ and $\alpha_0(^1\text{S}_0)$ are the polarizabilities of the 6^1S_0 and 6^3P_1 states of Hg atoms, respectively. Since $(\alpha_S^{\text{L}} - \alpha_S^{\text{H}}) = 0.9 \text{ \AA}^3$ and $[\alpha_0(^3\text{P}_1) - \alpha_0(^1\text{S}_0) = 3.95 \text{ \AA}^3]$ ⁴⁰⁾ are of the same order of magnitude, the magnitude of the measured band-gap shift is reasonable. In addition, since $\alpha_S^{\text{L}} - \alpha_S^{\text{H}} \ll \alpha_S^{\text{H}}$, the validity of the relation $\alpha_S^{\text{L}} \sim \alpha_S^{\text{H}}$ assumed above is confirmed.

The solid and dashed lines in Fig. 8 show the theoretical electric-field dependence of the energy shifts of the excitons peaks, with and without the image charge effect, respectively. Here, we have determined the band-gap shifts so that the calculated E_2^{res} reproduces the measured E_2^{res} . The measured shifts of E_1^{res} and E_2^{res} agree well with the theoretical shifts only when the image charge effect is taken into account. A remarked increase in ΔE_1^b is attributable to the smaller Bohr radius of the 1s excitons that is markedly reduced by the image charge effect. Note that the blue shift of the 1s excitons is not reproduced without the image charge effect. We thus conclude that the seemingly unique blue shift of the 1s exciton is due to the large reduction in exciton binding energy exceeding that of the band gap, on which the image charge effect plays an important role.

5. Conclusions

We have investigated the electronic and excitonic properties of an inorganic–organic perovskite-type quantum-well crystal $(\text{C}_4\text{H}_9\text{NH}_3)_2\text{PbBr}_4$ by absorption, photoluminescence, electroabsorption, two-photon absorption, and magnetoabsorption spectroscopies. The electronic structures of $(\text{C}_4\text{H}_9\text{NH}_3)_2\text{PbBr}_4$ are essentially the same as those of $(\text{C}_6\text{H}_{13}\text{NH}_3)_2\text{PbI}_4$, while the whole structures in $(\text{C}_4\text{H}_9\text{NH}_3)_2\text{PbBr}_4$ are shifted to the higher-energy side than those in $(\text{C}_6\text{H}_{13}\text{NH}_3)_2\text{PbI}_4$. Excitons in $(\text{C}_4\text{H}_9\text{NH}_3)_2\text{PbBr}_4$ are of the Wannier type, which is also the same as those in $(\text{C}_6\text{H}_{13}\text{NH}_3)_2\text{PbI}_4$. The exciton binding energy is markedly increased by two-dimensional spatial confinement and the image charge effect. The electronic and excitonic structures have been discussed in terms of group theoretical considerations, which explain well the observed absorption and photoluminescence spectra. Below Γ_5^- excitons that have a huge oscillator strength, we have found Γ_2^- and Γ_1^- excitons,

which have different selection rules. They are split by strong exchange interactions between the electron and the hole, which are strongly enhanced by the spatial confinement and image charge effect. The larger exciton binding energy, longitudinal–transverse splitting, exchange energy, and smaller enhancement factor caused by the image charge effect in $(\text{C}_4\text{H}_9\text{NH}_3)_2\text{PbBr}_4$ than $(\text{C}_6\text{H}_{13}\text{NH}_3)_2\text{PbI}_4$ are well explained by the fact that the dielectric constant of the well layer in $(\text{C}_4\text{H}_9\text{NH}_3)_2\text{PbBr}_4$ is smaller than that in $(\text{C}_6\text{H}_{13}\text{NH}_3)_2\text{PbI}_4$. We have observed a unique blue shift of the 1s exciton under applied electric fields perpendicular to the quantum-well layer. We have demonstrated with calculations that this blue shift of the 1s excitons is clear experimental evidence of the image charge effect on excitons.

Acknowledgements

This work was partially supported by Core Research for Evolutional Science and Technology (CREST), Japan Science and Technology Corporation, Japan.

- 1) T. Ishihara: in *Optical Properties of Low-Dimensional Materials*, eds. T. Ogawa and Y. Kanemitsu (World Scientific, Singapore, 1995) Chap. 6.
- 2) M. Hirasawa, T. Ishihara and T. Goto: *J. Phys. Soc. Jpn.* **63** (1994) 3870.
- 3) T. Ishihara, J. Takahashi and T. Goto: *Phys. Rev. B* **42** (1990) 11099.
- 4) T. Kataoka, T. Kondo, R. Ito, S. Sasaki, K. Uchida and N. Miura: *Phys. Rev. B* **47** (1993) 2010.
- 5) K. Tanaka and T. Kondo: *Sci. Tech. Adv. Mater.* **4** (2003) 599.
- 6) K. Tanaka, R. Ozawa, T. Kondo, T. Umabayashi, K. Asai and K. Ema: *Physica E* **25** (2004) 378.
- 7) L. V. Keldysh: *Pis'ma Zh. Eksp. Teor. Fiz.* **29** (1979) 716 [*JETP Lett.* **29** (1979) 658].
- 8) E. Hanamura, N. Nagaosa, M. Kumagai and T. Takagahara: *J. Mater. Sci. Eng.* **1** (1988) 255.
- 9) X. Hong, T. Ishihara and A. V. Nurmikko: *Phys. Rev. B* **45** (1992) 6961.
- 10) K. Tanaka, F. Sano, T. Takahashi, T. Kondo, R. Ito and K. Ema: *Solid State Commun.* **122** (2002) 249.
- 11) K. Tanaka, T. Takahashi, Y. Nabeshima, T. Kondo, R. Ito, T. Umabayashi, K. Asai and K. Ema: *Phys. Rev. B* **71** (2005) 045312.
- 12) T. Kondo, S. Iwamoto, S. Hayase, K. Tanaka, J. Ishi, M. Mizuno, K. Ema and R. Ito: *Solid State Commun.* **105** (1998) 503.
- 13) M. Era, S. Morimoto, T. Tsutsui and S. Saito: *Appl. Phys. Lett.* **65** (1994) 676.
- 14) K. Shibuya, M. Koshimizu, Y. Takeoka and K. Asai: *Nucl. Instrum. Methods Phys. Res., Sect. B* **194** (2002) 207.
- 15) J. Ishi, H. Kunugita, K. Ema, T. Ban and T. Kondo: *Phys. Rev. B* **63** (2001) 073303.
- 16) J. Ishi, H. Kunugita, K. Ema, T. Ban and T. Kondo: *Appl. Phys. Lett.* **77** (2000) 3487.
- 17) K. Ema, J. Ishi, H. Kunigita, T. Ban and T. Kondo: *Opt. Quantum Electron.* **33** (2001) 1077.
- 18) Y. Tabuchi, K. Asai, M. Rikukawa, K. Sanui and K. Ishigure: *J. Phys. Chem. Solids* **61** (2000) 837.
- 19) K. Tai, A. Mysyrowicz, R. J. Fischer, R. E. Slusher and A. Y. Cho: *Phys. Rev. Lett.* **62** (1989) 1784.
- 20) T. Goto, S. Taguchi and K. Cho: *J. Phys. Soc. Jpn.* **59** (1990) 773.
- 21) K. Tanaka: Dr. Thesis, The University of Tokyo, Tokyo, 2003.
- 22) Y. Kato, D. Ichii, K. Ohashi, H. Kunugita, K. Ema, K. Tanaka, T. Takahashi and T. Kondo: *Solid State Commun.* **128** (2003) 15.
- 23) D. E. Aspnes: in *Handbook on Semiconductors*, ed. M. Balkanski (North-Holland, Amsterdam, 1980) Vol. 2, p. 109.
- 24) D. A. B. Miller, D. S. Chemla, T. C. Damen, A. C. Gossard, W. Wiegmann, T. H. Wood and C. A. Burrus: *Phys. Rev. Lett.* **53** (1984) 2173.
- 25) K. Tanaka, T. Takahashi, T. Ban, T. Kondo, K. Ema, K. Uchida and N. Miura: *Solid State Commun.* **127** (2003) 619.
- 26) M. Shinada and S. Sugano: *J. Phys. Soc. Jpn.* **21** (1966) 1936.
- 27) T. Umabayashi, K. Asai, T. Kondo and A. Nakao: *Phys. Rev. B* **67** (2003) 155405.
- 28) Y. Nagamune, S. Takeyama and N. Miura: *Phys. Rev. B* **43** (1991) 12401.
- 29) R. Bonneville and G. Fishman: *Phys. Rev. B* **22** (1980) 2008.
- 30) D. Ichii, K. Kato, K. Ohashi, H. Kunugita, K. Ema, K. Tanaka, T. Takahashi and T. Kondo: 5th Int. Conf. Excitonic Processes Condensed Matter (EXCON), 2002.
- 31) W. Ekardt, K. Losch and D. Bimberg: *Phys. Rev. B* **20** (1979) 3303.
- 32) B. Sermage and G. Fishman: *Phys. Rev. B* **23** (1981) 5107.
- 33) W. Staudé: *Phys. Lett. A* **29** (1969) 228.
- 34) E. A. Muljarov, S. G. Tikhodeev, N. A. Gippius and T. Ishihara: *Phys. Rev. B* **51** (1995) 14370.
- 35) L. V. Kulik, V. D. Kulakovskii, M. Bayer, A. Forchel, N. A. Gippius and S. G. Tikhodeev: *Phys. Rev. B* **54** (1996) R2335.
- 36) A. D. Becke: *Phys. Rev. A* **38** (1988) 3098.
- 37) W. Stevens, H. Basch and J. Krauss: *J. Chem. Phys.* **81** (1984) 6026.
- 38) M. J. Frisch *et al.*: *Gaussian 98*, Revision A.7, Gaussian Inc., Pittsburgh, PA (1998).
- 39) X. Zhang, Y. Li, X. Kong and C. Wei: *Phys. Rev. B* **49** (1994) 10432.
- 40) D. M. Harber and M. V. Romalis: *Phys. Rev. A* **63** (2001) 013402.